Tropical tropospheric ozone morphology and seasonality seen in satellite and in situ measurements and model calculations

Jae H. Kim[1] and Sunmi Na

Department of Atmospheric Science, Pusan National University, Busan, Republic of Korea

M. J. Newchurch

Atmospheric Science Department, University of Alabama in Huntsville, Huntsville, Alabama, USA

R. V. Martin

Department of Physics and Atmospheric Science, Dalhousie University, Halifax, Nova Scotia, Canada

[1] An important issue in satellite remote sensing techniques for retrieving tropical tropospheric ozone is understanding the cause of the disagreement between ozone derived from satellite residual-based methods and the precursor distributions seen in both the fire count distribution and the Measurements Of Pollution In The Troposphere (MOPITT) CO distribution over northern tropical Atlantic and Africa in boreal winter and spring. This discrepancy has been called the Northern Atlantic paradox; however, it actually extends eastward all the way to Indonesia. We define the disagreement as the northern tropical paradox. We employ the scan angle method (SAM) to solve the paradox. This algorithm takes advantage of the difference in the Total Ozone Mapping Spectrometer (TOMS) retrieval information between nadir and high viewing angles. The averaging kernel for this difference exhibits a broad maximum centered at $\sim$5 km in the troposphere and thereby can be used to estimate tropospheric ozone information. The seasonal distribution of tropospheric ozone derived from the SAM algorithm shows remarkably good agreement with fire counts from Along Track Scanning Radiometer (ATSR), CO from MOPITT, TOMS aerosol index, and ozone distribution from the GEOS-CHEM model in four seasons over the tropics. In meridional distribution, all of these products clearly reveal the seasonal oscillation between northern tropical Africa in boreal winter and over southern tropical Africa in boreal summer. The residual-based methods (TOR, CCD, CCP, and modified residual), however, always show the ozone maximum over the southern Atlantic off the coast of southwest Africa. A further comparison with the in situ measurements from the Measurement of Ozone and Water Vapor by Airbus In-Service Aircraft (MOZAIC) campaign at three locations over the northern tropics, Abidjan (5°N, 4°W), Madras (13°N, 80°E), and Bangkok (14°N, 101°E), supports our results. The seasonality of ozone from the SAM and the model, which shows the ozone maximum in boreal summer and the minimum in boreal winter, is in accordance with the MOZAIC measurements. However, the seasonality of the RBMs does not agree with the seasonality of in situ measurements. We conclude that the northern tropical paradox does not actually exist.

---

[1]Also at Atmospheric Science Department, University of Alabama in Huntsville, Huntsville, Alabama, USA.

1. Introduction

[2] Tropospheric ozone plays an important role in controlling atmospheric chemical composition and affects global climate and air quality. There has been a demand for a satellite sensor specifically designed to detect tropospheric ozone with high spatial and temporal resolution.

However, because stratospheric ozone, about 90% of the total ozone column, is located above tropospheric ozone, it is difficult to measure tropospheric ozone directly from a satellite, and current tropospheric ozone retrieval algorithms have been only partially successful.

[3] The residual method is an indirect method that subtracts the stratospheric ozone column measured by various satellites from Total Ozone Mapping Spectrometer (TOMS) total ozone column measurements. These methods are the tropospheric ozone residual (TOR) method [*Fishman and Larsen*, 1987], the convective cloud differential (CCD) method [*Ziemke et al.*, 1998], the modified residual method [*Hudson and Thompson*, 1998; *Thompson and Hudson*, 1999] and the clear cloudy pairs (CCP) method [*Newchurch et al.*, 2003]. The common assumption made by these methods, except by CCP, is that stratospheric ozone is zonally invariant in the tropics. However, *Kim and Newchurch* [1996] and *Newchurch et al.* [2001] have suggested that stratospheric ozone variation is also responsible for part of the wave-one pattern that appears in TOMS total ozone in the tropics with a maximum over the Atlantic and a minimum over the Pacific Ocean. The CCP method allows for this zonal variance when it is present in the TOMS cloudy measurements. Otherwise, the magnitude of the zonal deviation from the flat stratospheric ozone assumption will propagate directly into the tropospheric ozone column of the residual-based methods (RBMs). Topographic contrast methods [*Jiang and Yung*, 1996; *Kim and Newchurch*, 1996, 1998] derive tropospheric ozone below mountain tops in the lower 2–3 km of the troposphere.

[4] The distributions of tropospheric ozone from the RBMs have shown a persistent maximum over the southern tropical Atlantic for all months of the year, and it was suggested that biomass burning is responsible for the elevated ozone. However, the fire atlas from Along Track Scanning Radiometer (ATSR) shows an annual north to south oscillation of burning activities, with considerable biomass burning activity over northern Africa for December–February, and over southern tropical Africa for June–September. Therefore a serious contradiction exists between the seasonal distribution of tropospheric ozone and fire count distribution. This puzzling disagreement between the RBMs products and fire counts has been called the tropical Atlantic paradox [*Thompson et al.*, 2000].

[5] From comparisons between CCD, in situ measurements over northern tropical regions, and the Goddard Earth Observing System chemical transport model (GEOS-CHEM) calculations, *Martin et al.* [2002] showed that the difference between CCD and model output as well as in situ measurements occurs not only over northern Africa, but also over southern Asia (hereinafter northern tropical paradox). *Edwards et al.* [2003] used Measurements Of Pollution In The Troposphere (MOPITT) CO, fire counts, and Model for Ozone And Related chemical Tracers (MOZART) calculations to understand the tropospheric ozone features in tropical tropospheric ozone from the various tropical tropospheric O_3 column products. They found inconsistencies between the products obtained from Earth Probe (EP) TOMS data, and between these products, in situ measurements, and modeling results. The Geophysical Fluid Dynamics Lab three-dimensional global chemical transport model [*Galanter et al.*, 2000] also shows the ozone maximum over northern Africa during boreal winter. If the evidence from these studies is credible, we must consider whether the northern tropical paradox really exists or is an artifact of the RBMs.

[6] Currently, the only satellite-based measurements of tropospheric ozone that show consistent seasonality with the fire counts (http://www.atsr.rl.ac.uk/) and MOPITT CO (http://www.eos.ucar.edu/mopitt) are the products from the scan angle method (SAM), which was applied to TOMS data for the year of 1997 as a case study [*Kim et al.*, 2001]. In this paper, we start with the physical meaning and limitations of SAM-derived tropospheric ozone index (TOI), then discuss ways to improve its data quality, followed by a comparison of the TOI with various data such as satellite observations of CO from MOPITT, fire counts from ATSR, ozonesonde measurements from Southern Hemisphere Additional Ozonesondes (SHADOZ), in situ profiles from Measurement of Ozone and Water Vapor by Airbus In-Service Aircraft (MOZAIC), TOMS aerosol index (AI), products from the GEOS-CHEM, and RBMs-derived tropospheric ozone. Because the issue of the northern tropical paradox is associated with both the geographical distribution and the seasonality of tropospheric ozone, we focus on identifying the differences in spatial and temporal distributions between various measurements. Then, we discuss possible clues about the occurrence of the northern tropical paradox. In this study, we have used only version 7 level 2 TOMS data under clear-sky conditions from August 1996 to December 2000 because TOMS data contain a noticeable error after 2000 [*McPeters*, 2003]. We have not used version 8 TOMS data because that version employs a variable a priori tropospheric profile and the SAM takes advantage of deviations from a fixed a priori. Our V7 data has been corrected for the TOMS scan-dependent error due to aerosol loading and sunglint effect, which is nearly the same correction algorithm applied to version 8 TOMS data.

2. Scan Angle Method (SAM)

[7] TOMS measures backscattered UV radiances while scanning across the orbital track. With known atmospheric characteristics, measured radiances depend on ozone amounts and the ozone vertical distribution. When the sky is clear, the effective reflecting surface due to atmospheric Rayleigh scattering varies from the lower troposphere to the upper troposphere depending on solar zenith angle and satellite viewing angle. At a given solar zenith angle, the backscattered photons observed at nadir and high-scan positions have seen the same amount of stratospheric ozone, but different amounts of tropospheric ozone because of different altitudes of the effective reflecting surface. This phenomenon causes the TOMS algorithm to produce a known error in the retrieved total ozone associated with the TOMS viewing angles. The sign and magnitude of the error is proportional to the difference between actual tropospheric ozone and the a priori tropospheric ozone amount in the algorithm. For instance, if the a priori tropospheric ozone amount is smaller than actual amount, the retrieved total ozone will be an underestimate of the actual amount and the retrieved total ozone at nadir will be higher than the ozone at high viewing angle. An important point is that the
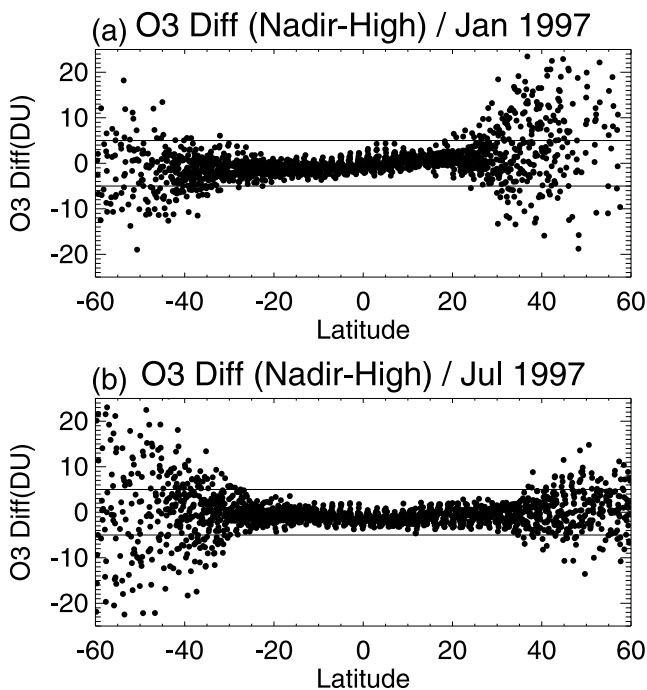
Figure 1. Latitudinal variation of the total ozone difference between nadir and high-scan positions in (a) January and (b) July 1997.

sign of total ozone difference between nadir and high viewing angles becomes positive and the magnitudes of the difference will be proportional to the magnitudes of the difference between the a priori and the actual tropospheric ozone amount. On the other hand, if the a priori tropospheric ozone amount is larger than actual amount, the error goes in the opposite direction. Thereby, the sign of total ozone difference between nadir and high viewing angles becomes negative and the magnitude of the difference will also be proportional to the magnitudes of the difference between the a priori and the actual tropospheric ozone amount, which is the difference in tropospheric ozone retrieval efficiency. The calculated averaging kernel for the difference between TOMS nadir and high viewing angles maximizes in the troposphere with a peak near an altitude of 5 km [*Kim et al.*, 2001]. This analysis suggests that the total ozone difference between two viewing angles contains information about tropospheric ozone. We define this difference as the tropospheric ozone index. Because the actual tropospheric ozone amount between 0 and 60 DU corresponds to the TOI values of −5 and +5, respectively, the appearance of the TOI value beyond this range exceeds the application limit of this method. We use this range as a diagnostic metric to identify the applicable domain of the SAM results. Because the a priori tropospheric ozone in the TOMS V7 algorithm is about 32 DU, the positive and negative TOI values represent tropospheric ozone amounts more or less than 32 DU, respectively.

[8] Because the TOMS, which is a cross-track scanning sensor, does not measure simultaneously at nadir and high viewing angles, the TOI from TOMS data cannot be determined in a single orbit. However, the TOMS orbital track drifts about 5° in longitude each orbit, and so the

measurements at nadir overlap with those at high viewing angle 2−3 days later. Then, two factors contribute to the total ozone difference between the viewing angles ($\Delta\Omega$) because the measurements do not occur at the same time.

$$\Delta\Omega = \text{TOI} + \text{SOD} \qquad (1)$$

SOD is the stratospheric ozone differences between 2−3 days interval. We have selected a 2° latitude by 15° longitude region, which is large enough to obtain many measurements both at nadir and at high scan positions and small enough to eliminate SOD. Because daily variation of stratospheric ozone over the TOMS footprint of about of 100 km × 50 km stratospheric ozone could be sudden and large, we have to examine if the contribution of the SOD is averaged out from this procedure by analyzing the diagnostic metric to constrain results where the TOI value is within +5 and −5.

[9] Figure 1 shows TOI values in January and July as a function of latitude averaged over 1997−2000. The TOI values beyond the criterion of ±5 are frequently observed as the latitude increases. This pattern is consistent with stratospheric ozone variation that is strong and active in higher latitudes especially in the winter hemisphere. Therefore the application of the SAM is limited in the latitude bands between 15°S to 15°N extended to 35° latitude in the summer hemisphere where the influence of the SOD is small.

[10] Figure 2a shows the derived TOI in July averaged over 1997−2000, and Figure 2b shows the CO in July 2000 from MOPITT. Very low ozone is observed over the remote Pacific Ocean, the Indian Ocean, and the Atlantic Ocean, while elevated ozone is observed over Africa associated
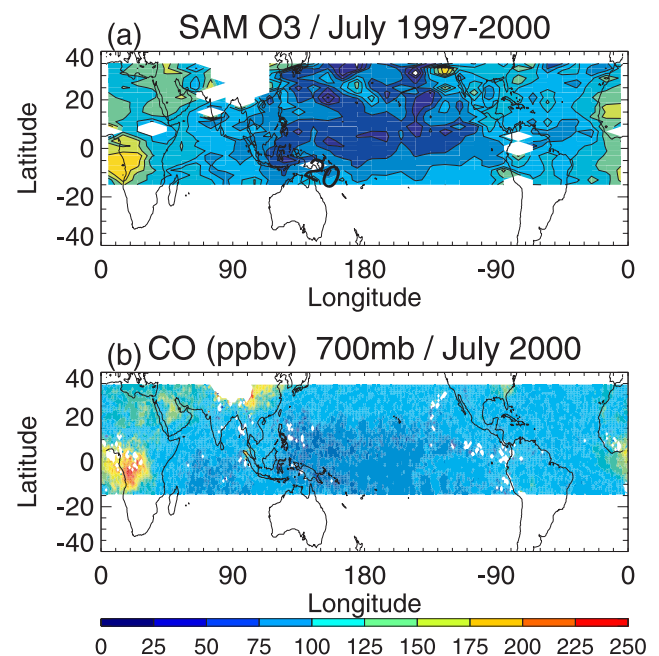

Figure 2. Distribution of (a) tropospheric ozone column (DU) derived from SAM for July from 1997 to 2000 and (b) CO measured from MOPITT for July 2000. White space between 15°S and 35°N shows cloudy regions.
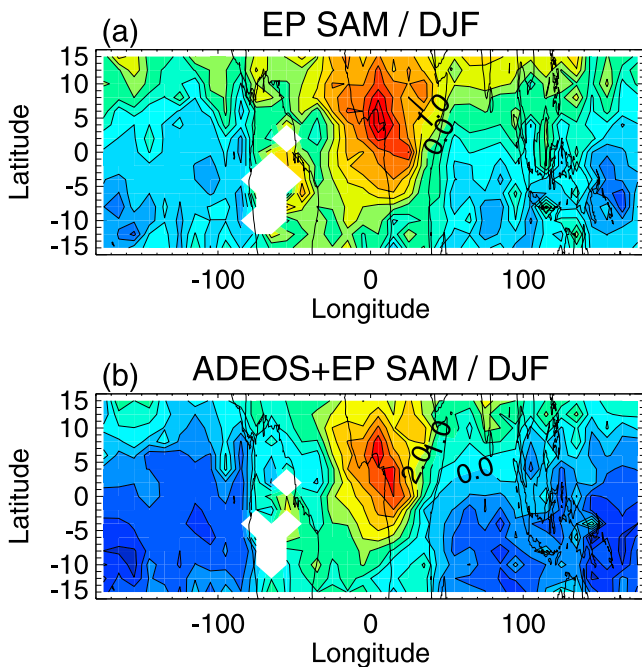
Figure 3. Distribution of tropospheric ozone index derived from (a) the EP-only SAM and (b) the ADEOS + EP SAM for December 1996 to February 1997.

with biomass burning activity, over Saudi Arabia possibly associated with a complex interplay of transport and chemistry, and over northeast Asia associated with industrial plume from China [*Li et al.*, 2001]. Relatively moderate elevation of tropospheric ozone is observed over North and South America. These distributions appear to match well with the source regions of tropospheric ozone as well as CO distribution, an ozone precursor.

[11] In order to reduce the contribution from SOD, and unknown random errors in equation (1), it is very important to have enough measurements both at nadir and at high viewing angles. Figure 3a shows the TOI distribution with only EP TOMS data averaged from December 1996 to February 1997, which corresponds to the northern tropical biomass-burning season. Amounts of tropospheric ozone over northern tropical regions are higher than over southern tropical regions, and a maximum is observed over northern Africa and the adjacent Atlantic Ocean. The lowest ozone amounts are observed over the Indian and Pacific Oceans. When we combine EP TOMS data with Advanced Earth Observing Satellite (ADEOS) TOMS data, which has a record only from September 1996 to June 1997, the overall patterns remain, but a significant reduction of the noise is observed over the remote regions (Figure 3b).

3. Analysis

3.1. Morphology of Tropical Tropospheric Ozone

[12] The evaluation of satellite products typically proceeds through comparison of those products with ozonesonde measurements over a small number of ozonesonde stations mostly in the southern tropics. None of the methods performs badly in the comparison [*Kim et al.*, 2001; *Chandra et al.*, 2002; *Newchurch et al.*, 2003; *Thompson*

et al., 2003]. However, because the issue of the northern tropical paradox has been raised as the inconsistency between the seasonality of satellite-derived tropospheric ozone and of biomass burning, it is hard to decide if one method is better than the other based on the agreement with a few sonde stations in the other hemisphere. The evaluation of the satellite products must be performed based on not only local in situ observations, but also on a global perspective in order to resolve the northern tropical paradox. However, there is insufficient coverage by ground stations for the evaluation of the satellite products from a global perspective. We use TOMS AI, fire counts from ATSR, CO (an ozone precursor) from MOPITT, and chemical transport model products [*Crutzen and Andreae*, 1990; *Singh*, 1995; *Galanter et al.*, 2000]. The chemical transport model used here is from the GEOS-CHEM model described in Appendix A [*Bey et al.*, 2001; *Martin et al.*, 2002].

[13] For this purpose, we begin by converting the TOI into tropospheric ozone column amount according to theoretical basis discussed by *Kim et al.* [2001], which is $6.7 \times$ TOI + 32 DU. Remember that the averaging kernel of the TOI has a maximum at 5 km and thereby the converted ozone amounts are not the actual tropospheric ozone column, but the tropospheric ozone column weighted according to the kernel.

[14] Figures 4a, 4b, and 4c show fire counts from ATSR, TOMS AI averaged over 1996–2000, and MOPITT CO measurements for only 2000, respectively. They show that enhanced CO and TOMS AI are mainly produced by biomass burning activity in the tropics. Figure 4d shows tropical tropospheric ozone derived from the SAM for December–February (DJF) period, which is the biomass-burning season in the northern tropics, averaged over 1996–2000. The SAM products show a distinctive maximum over northwest equatorial Africa, and the ozone amounts over the northern tropics are significantly higher than over the southern tropics. The elevated ozone over South America and marginally elevated ozone over Indonesia and northern Australia are also consistent with the CO distribution. Figure 4c remarkably resembles Figure 4d in the east-west distribution as well as north-south distribution. However, CCD-derived tropospheric ozone over the same period shows a maximum over the southern Atlantic and higher ozone over the southern tropics than over the northern tropics (Figure 4e). The clear cloudy pairs method (http://www.nsstc.uah.edu/atmchem/toms_tropos_ozone/toms_ozone.html) [*Newchurch et al.*, 2003], which is of the heritage of CCD but allows the zonal wave-one variation for stratospheric ozone instead of using invariant stratospheric ozone and also uses all cloudy observations, not just Western Pacific clouds, also derives a distribution similar to the CCD. These features are significantly different from the fire counts and the MOPITT CO distribution. The ozone distribution from the GEOS-CHEM model calculation for 1996–1997 in Figure 4f shows a similar north-south gradient to that from the SAM.

[15] The features of fire counts, TOMS AI, and CO distribution for the March–May (MAM) period are about the same as of those for the DJF period, but the intensities have decreased in Figures 5a, 5b, and 5c. This decrease occurs because the biomass burning activity is the strongest in the DJF period, and then starts to diminish and finally
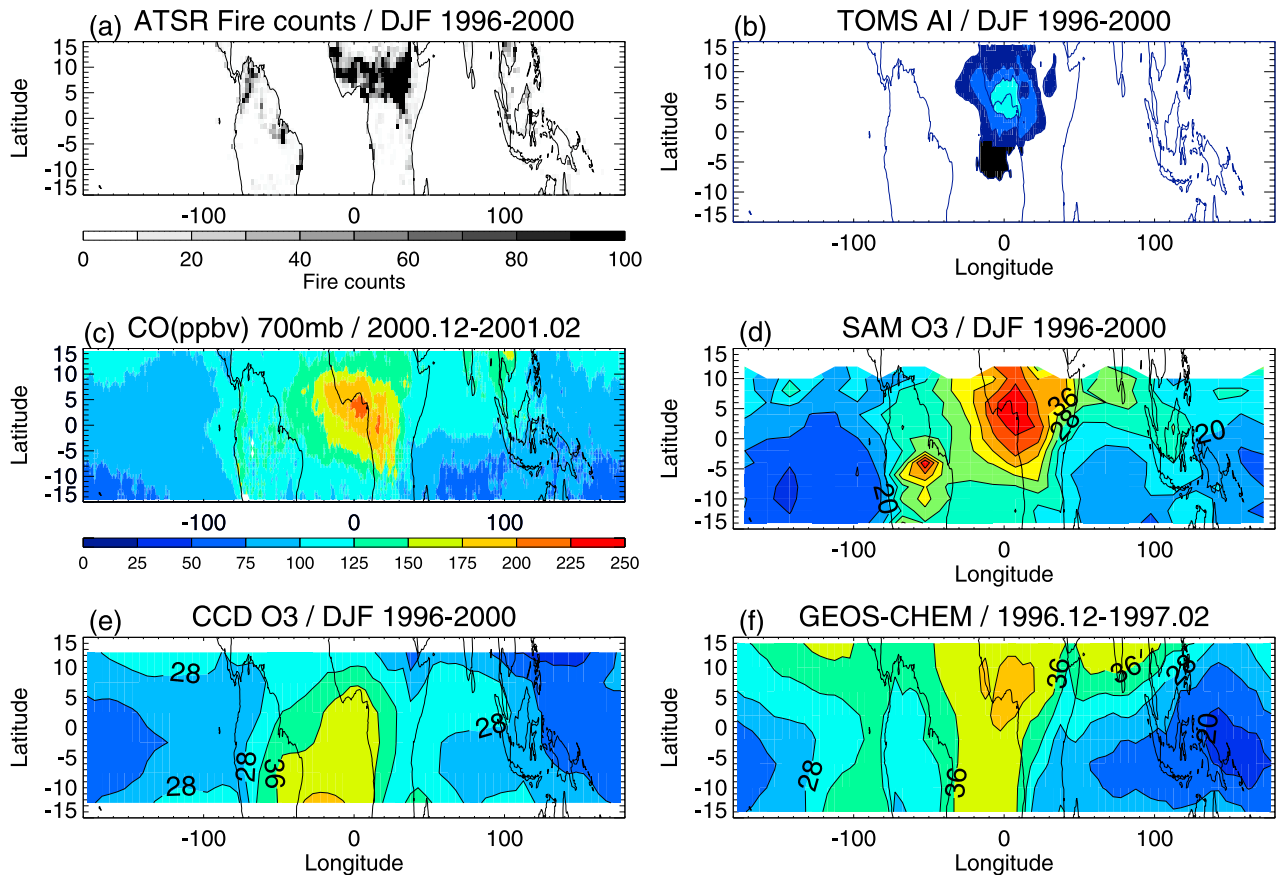
Figure 4. Distribution of (a) fire counts from ATSR averaged for 1996–2000, (b) aerosol index from TOMS averaged for 1996–2000, (c) CO from MOPITT for 2000, (d) tropospheric ozone column (DU) from SAM averaged for 1996–2000, (e) tropospheric ozone column (DU) from CCD averaged for 1996–2000, and (f) tropospheric ozone column (DU) from GEOS-CHEM model for 1997 in the December-January-February time period.

ends around in May over the northern tropics (http://shark1.esrin.esa.it/ionia/FIRE/AF/ATSR/). The AI maximum is observed north of the CO maximum. Because both biomass-burning and dust aerosols contribute to the TOMS AI distribution while only biomass-burning aerosols are related to the CO distribution, the AI maximum at the northern edge is likely due to the influence of dust aerosols from the Sahara desert. The features of the ozone distribution from the SAM in the MAM period are the same as in the DJF period with decreasing ozone amounts and a north-south gradient as in the fire counts, AI, and CO. However, the ozone maximum from the CCD has changed only from the south central Atlantic to the equatorial Atlantic. The comparison of the model products with the SAM products reveals remarkably good agreement in zonal ozone distribution as well as meridional distribution; although the model derives the maximum ozone over India while the SAM over northwest equatorial Africa.

[16] As the burning season starts over the southern tropics in June, the biomass-burning activity migrates toward the southern tropics and intensive burning occurs over South America and South Africa as seen in Figures 6a and 6c. The TOMS AI shows two maxima; one over southern Africa due to biomass-burning aerosol, and the other in sub-Saharan Africa due to dust aerosols. None of the burning

signal is detected over northern Africa corresponding to wet season. The number of fire counts in June–August (JJA) is higher than in September–November (SON) over southern Africa, while the fire count in the SON period is higher than in the JJA period over South America. The SAM, the CCD, and the model products commonly show the ozone maximum over southern Africa and the adjacent Atlantic, which is consistent with fire counts and CO measurements. It is noticeable that the intrusion of low ozone originating from the western Pacific and crossing the Indian Ocean to northern equatorial Africa in Figure 6d remarkably resembles the ozone distribution in Figure 6f.

[17] The strongest biomass-burning activity is not observed over southern Africa but over South America in the SON period 1996–2000 in Figure 7a. However, the TOMS AI is closer to South America and the CO concentrations are higher in Africa for year 2000. The differences between fire counts and CO could be due to different years of coverage between two data sets. A significant number of fire counts observed over northern Africa for the SON period must be due to the onset of biomass-burning activity in November (http://shark1.esrin.esa.it/ionia/FIRE/AF/ATSR/). The SAM tropospheric ozone distribution in Figure 7d shows the highest ozone over South America coincident with the fire counts. The ozone
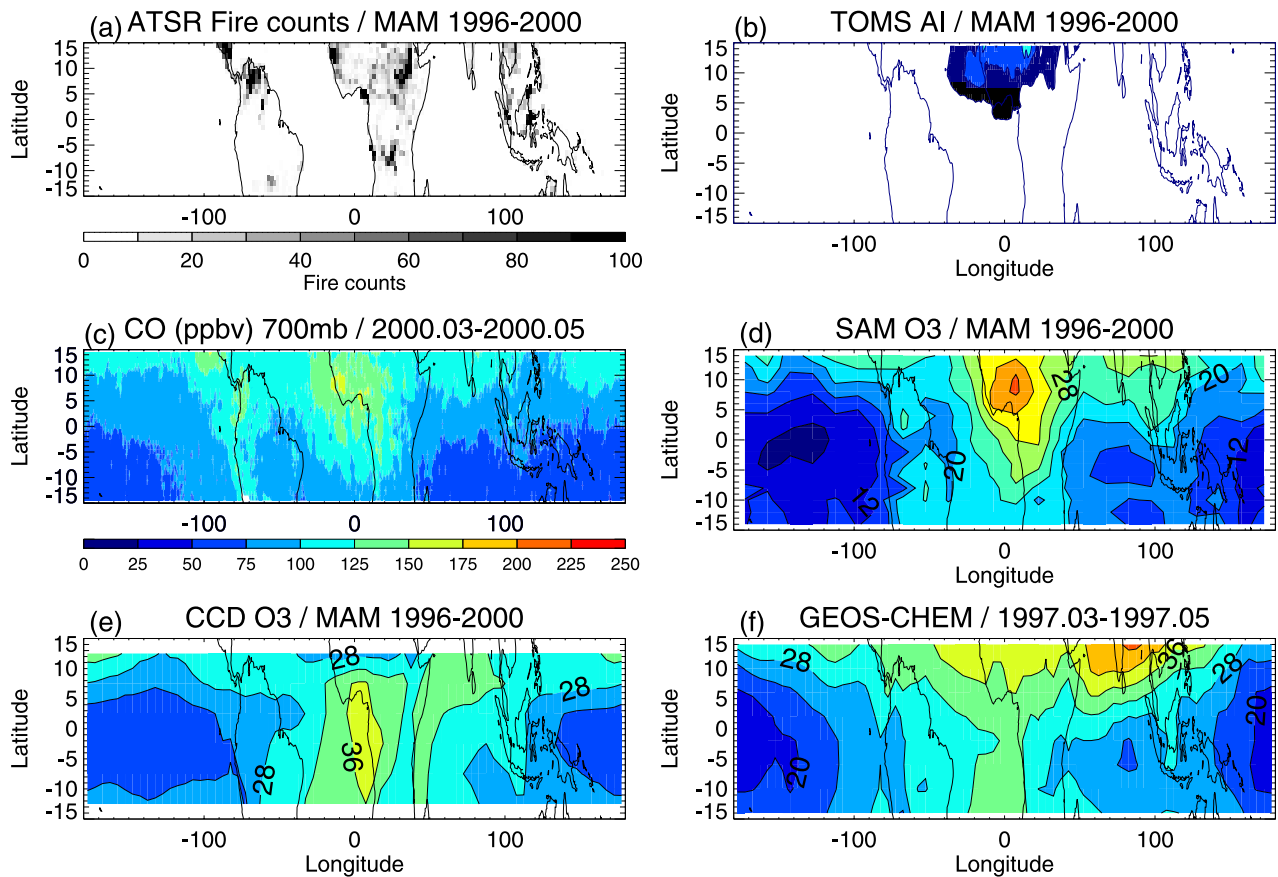
Figure 5. As in Figure 4, but in the March-April-May time period.

over southern Africa is smaller than in the previous season. This tendency also agrees with the decrease of the total number of fire counts in the JJA period (17012) compared to the SON period (8967). On the other hand, the ozone over northern Africa is larger due to the onset of biomass burning starting as early as late October. The lowest ozone amounts are always observed over the Pacific Ocean for all products. It is of interest that ozone over the Indian Ocean shows a local minimum between Indonesia and Africa. This pattern is also observed in MOPITT CO and the GEOS-CHEM model while the CCD products show a rather gradual decreasing tendency from Africa across the Indian Ocean to the Pacific Ocean. It is reasonable to expect that the remote Indian Ocean is cleaner than Indonesia and Africa. The number of fire counts over Indonesia and Australia shows record high counts in four seasons (http://shark1. esrin.esa.it/ionia/FIRE/AF/ATSR/). The SAM products show marginally higher ozone in this season. There is no remarkable difference in the distribution between the SAM and the CCD for the SON period. The observed differences are that the CCD products do not show any significant change in distribution between the JJA and the SON period except that the ozone amounts are significantly increased over the southern Atlantic, and the increasing tendency of the north-south gradient over Africa and the Atlantic is opposite to that seen in the SAM products. The GEOS-CHEM products show a tendency similar to the CCD products over the southern Atlantic with widely elevated ozone over the

entire southern tropics. The elevated ozone over Indonesia in the model output is due to intensive burning in the El Nino event of 1997 (http://shark1.esrin.esa.it/ionia/FIRE/AF/ATSR/).

[18] The SAM products agree remarkably well with the patterns of fire counts and MOPITT CO. This agreement is consistent with various studies that biomass burning is the main source of tropical tropospheric ozone. The model products clearly show seasonal oscillation between northern and southern Africa in accordance with biomass-burning activity as do the SAM product; however, this oscillation has not been observed in the RBM products. Therefore there is no paradox between the SAM tropospheric ozone and the biomass burning activity.

[19] The significant difference between the RBMs products and biomass burning activity occurs in boreal winter and spring when the planetary activity is the strongest. In the lower stratosphere, planetary waves propagating into the tropics break in two westerly regions, the Pacific and the Atlantic [Horinouchi et al., 2000; Waugh and Polvani, 2000; Scott et al., 2001; Waugh and Funatsu, 2003]. In northern winter and spring, the strong planetary wave forcing may modulate O_3 fluctuations. Lower ozone is associated with transport of O_3-poor air from equatorial region, while higher ozone is associated with transport of O_3-rich air from high-latitude regions. This transport suggests that it is important to the analyses of tropical ozone to take into account the dynamical processes.
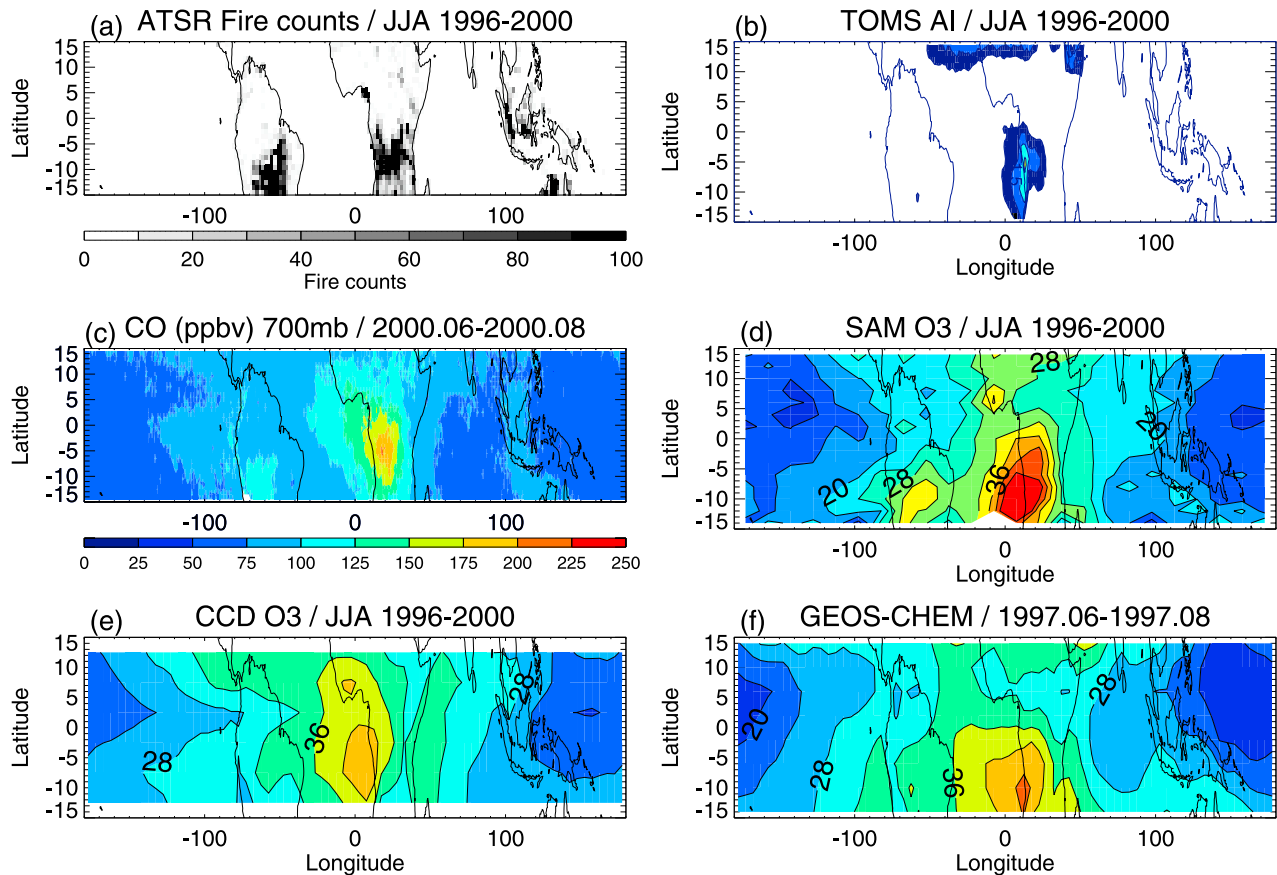
Figure 6. As in Figure 4, but in the June-July-August time period.

Because the common assumption made by the residual-based method is that stratospheric ozone is zonally invariant in the tropics, the strong planetary wave activity may produce a significant error in the RBMs products. Therefore dynamical influence of the strong planetary wave activity on tropical stratospheric ozone is possibly linked to the paradox from the RBM products. The SAM, however, is largely insensitive to stratospheric ozone variations.

3.2. Seasonality of Tropical Tropospheric Ozone

[20] There are limited ozonesonde data sets available in the tropics. However, the measurements at Natal (5°S, 35°W) and Ascension Island (8°S, 14°W) have been widely used for the purpose of validating the satellite-based retrieval method because of their relatively long records. Surprising differences have not been reported in the comparison of various satellite products with ozonesonde measurements over these southern equatorial regions [*Kim et al.*, 2001; *Chandra et al.*, 2002; *Martin et al.*, 2002; *Thompson et al.*, 2003]. Figure 8 shows a comparison of the CCD and the SAM products for 1996–2000 with SHADOZ ozone soundings for 1998–2002 at these stations. The SAM and the CCD products are averaged over 2° latitude × 15° longitude and 5° latitude × 5° longitude for 1996–2000 centered at the stations, respectively. Although neither the CCD nor the SAM products exactly matches the ozone soundings in absolute magnitude, the seasonality of these products occurs in general accord

with the seasonality of the soundings, which show high ozone in austral spring and low ozone in austral autumn.

[21] The primary interest in this paper is to describe the agreement in seasonality between SAM TOI and in situ measurements, and the possible clues about the existence of the Northern Tropical Paradox. For this purpose we have used in situ measurements from the Measurement of Ozone and Water Vapor by Airbus In-Service Aircraft (MOZAIC) campaign [*Marenco et al.*, 1998] along with GEOS-CHEM products. Figure 9 shows the monthly variation of SAM, CCD, MOZAIC, and GEOS-CHEM tropospheric ozone column at Abidjan (5°N, 4°W), Madras (13°N, 80°E), and Bangkok (14°N, 101°E) located in the northern tropics. Here the MOZAIC and the GEOS-CHEM-derived tropospheric ozone amounts are integrated from the surface to 200 mb, which is lower than the tropical tropopause of about 100 mb. Because the ozone amount between 200 mb and 100 mb is small [*Liu et al.*, 2003], the integrated ozone column up to 200 mb is adequate to investigate the seasonality of tropospheric ozone column while avoiding any potential stratospheric contamination. The variation of the SAM at Abidjan, in northwestern equatorial Africa, shows the ozone maximum for the DJF period consistent with the MOZAIC and the GEOS-CHEM, while the CCD shows a broad maximum from June to October (Figure 9a). Recall that the SAM product is weighted near 5 km altitude and the CCD products are integrated from the surface to the altitude of high clouds close to the tropopause. If missing data in September for the MOZAIC is restored by linear
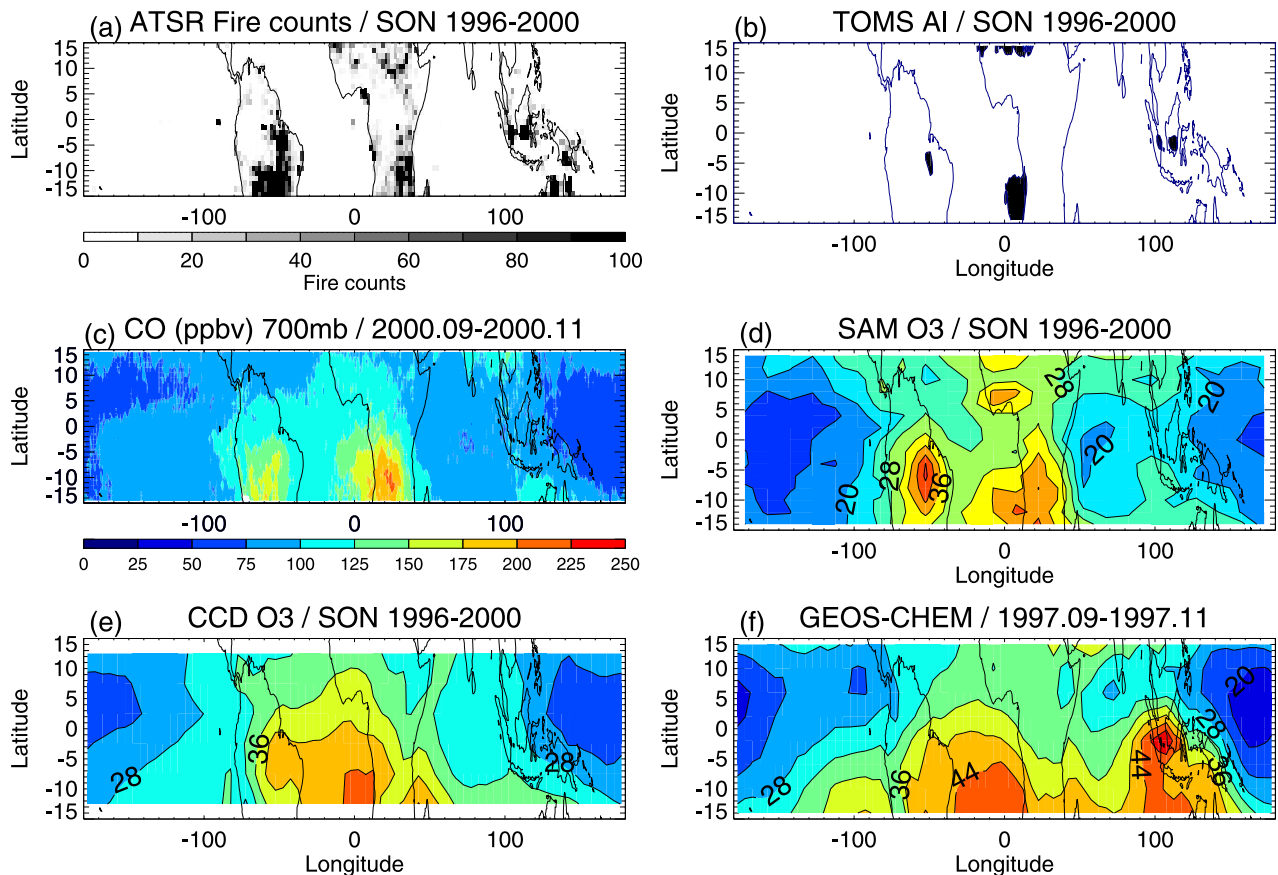
Figure 7. As in Figure 4, but in the September-October-November time period.

interpolation, the SAM, the MOZAIC, and the GEOS-CHEM exhibits the ozone minimum for August–September, for July–September, and September–October, respectively. However, the CCD method finds the minimum in January–March. Therefore the seasonality of the SAM is consistent with that of in situ ozone and fire counts measurements, but the seasonality of the CCD is completely opposite to the seasonality of these measurements in northern Africa.

[22] In Figure 9b the SAM products show the maximum ozone in December–January and the minimum from June to August, while the model and the MOZAIC products show a broad maximum from January to May and minimum in July–August in Madras, India. Even though the months of maximum do not exactly match, the tendency shows consistency; ozone maximum in boreal winter and spring and minimum in boreal summer. However, the CCD products show two maxima in boreal spring and autumn and two minima in winter and summer.

[23] Remarkably good agreement appears between the SAM, the MOZAIC, and the model in Bangkok, Thailand. The tendency of monthly variations corresponds well; maximum in boreal winter and minimum in boreal summer. This pattern is consistent with the ozone increase due to biomass burning activity in the dry season of winter and spring, and ozone decrease due to a reduction in the burning activity in the wet season of summer [*Pochanart et al.*, 2001; *Yonemura et al.*, 2002]. However, the CCD product

shows an out-of-phase tendency with the seasonality in Bangkok.

4. Comparison of SAM-Derived Tropospheric Ozone From Version 7 (V7) and Version 8 (V8)

[24] Recently, the V8 TOMS data has been released after including corrections with better profiles for ozone and temperature climatology, and for aerosols and seaglint effects. The V8 algorithm adjusts total ozone to be consistent with climatological total ozone and temperature profiles, which vary with latitude and month. The V8 data are also corrected for aerosol interference and seaglint effect. Because the TOMS a priori now varies with latitude and month, the SAM TOI and the conversion to DU from the V8 data will be somewhat different from the TOI and DU in the V7 data. A prerequisite for applying the SAM method is to use fixed a priori profiles for tropospheric ozone. Using the V8 algorithm ozone profiles that varying with latitude and month, requites a more complicated derivation. If the V7 data are used, we need to estimate the errors in climatological profiles for ozone and temperature, plus aerosols and seaglint effect.

[25] If the SAM is applied to total ozone data from the V7 and V8 algorithm, TOI values differ by (1) an offset due to tropospheric ozone retrieval efficiency difference in ozone profile between two algorithms and (2) the error due to aerosols and seaglint effect. The offset is constant in a given

month and latitude because the V8 algorithm uses the same correction procedure in a given month and latitude. Therefore the residual of TOI values from zonal mean must be the same in a given month and latitude. Figure 10 shows the comparison of the TOI residual derived from V7 and V8 data. Even though the regression coefficient is very good, small differences exist between the residual with V7 and V8. These differences result from aerosols and seaglint effect. The seaglint effect occurs only over oceans when the satellite-viewing angle is close to solar zenith. Because this research focuses on a climatological study with averages over long periods of time, the seaglint effect will be smoothed out because it does not have a favor for a particular time and region. In the comparison of various satellite measurements in section 3, we have shown that tropospheric ozone is closely linked to biomass burning, which is associated with aerosols. We have not found any pattern that is related to the seaglint effect over oceans. Therefore the difference between V7 and V8 TOI is mainly due to the aerosol interference. The expected error due to aerosol effect ranges from the lowest value of 0.46 for MAM period and the highest value of 0.76 for JJA period within 95% confidence intervals (c.i.) from Figure 10. These TOI values correspond to 3.1 DU (MAM) and 5.1 DU (JJA) using the conversion factor of 6.7. When these errors are applied to the derived tropospheric ozone map over biomass burning regions in Figures 4–7, the features of the ozone map remain unchanged because the tropospheric ozone amounts along zonal and meridional direction are well above the 2-sigma confidence interval. TOMS AI values are small over Ascen-

Figure 9. Monthly mean tropospheric ozone column (DU) from SAM (solid squares), the CCD method (crosses), the GEOS-CHEM model (solid circles), and the MOZAIC observations (open circles) over at (a) Abidjan (5°N, 4°W), (b) Madras (13°N, 80°E), and (c) Bangkok (14°N, 101°E).

sion Island, Natal, Madras, and Bangkok from Figures 4–7, while they are significantly higher over Abidjan during the DJF period. Therefore it is expected that aerosols influence the seasonality over Abidjan. However, because seasonal variation of SAM-derived ozone is about 20 DU over Abidjan, which is well above the 2-sigma error due to aerosols of 5.1 DU, we expect that this small error will not change the observed seasonality which displays a maximum in January and a minimum in September.

5. Conclusions

[26] An important issue in satellite remote-sensing techniques for retrieving tropical tropospheric ozone is resolving
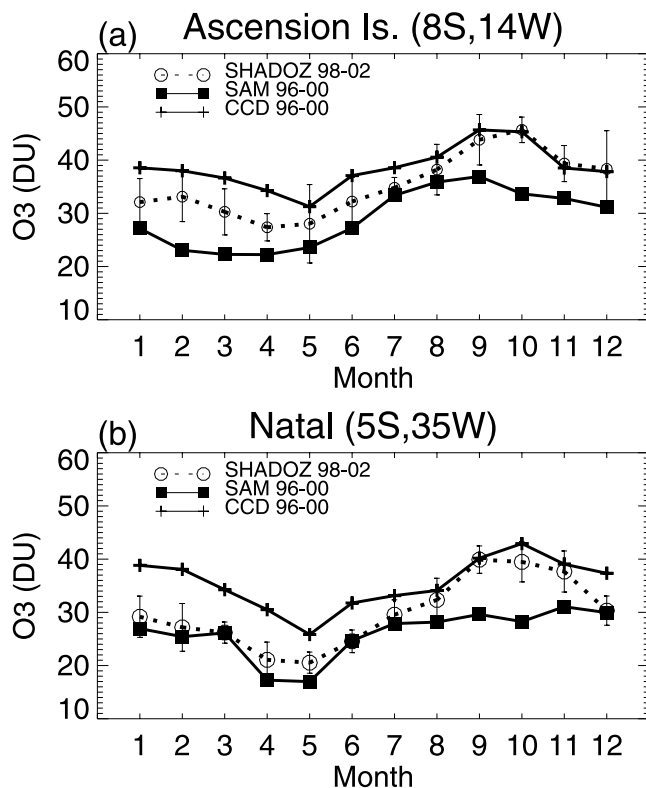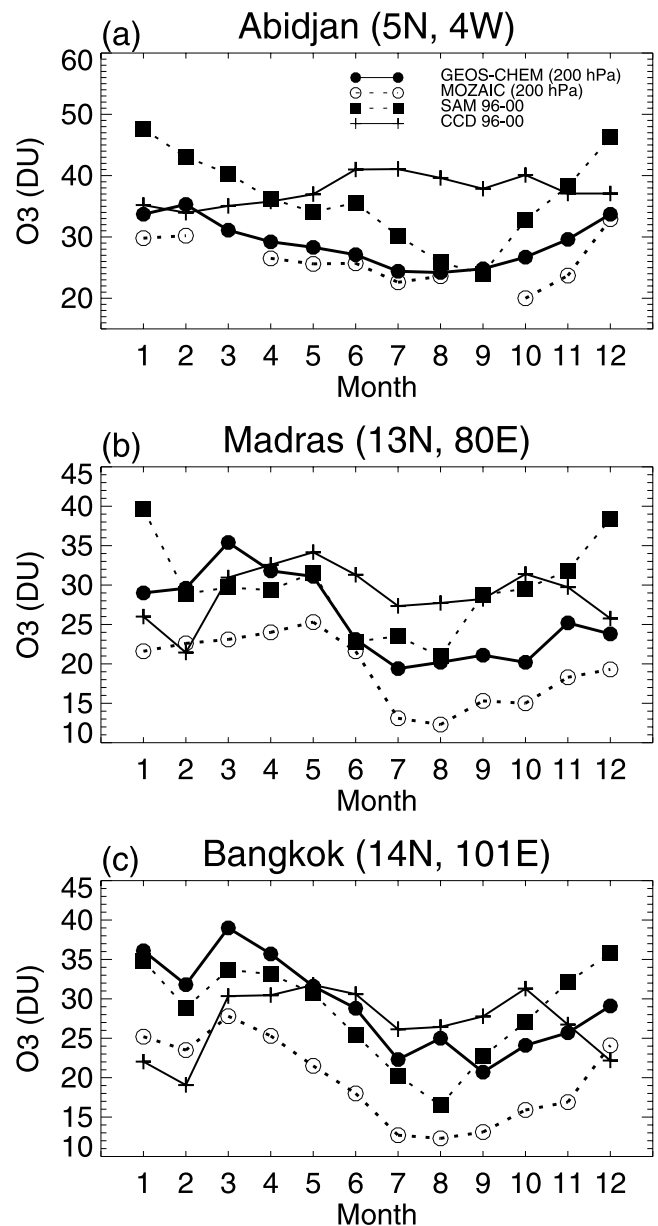

Figure 8. Monthly mean tropospheric ozone column (DU) from SAM (solid squares), the CCD method (crosses), and the SHADOZ measurements (open circles) at (a) Ascension Island (8°S, 14°W) and (b) Natal (5°S, 35°W).
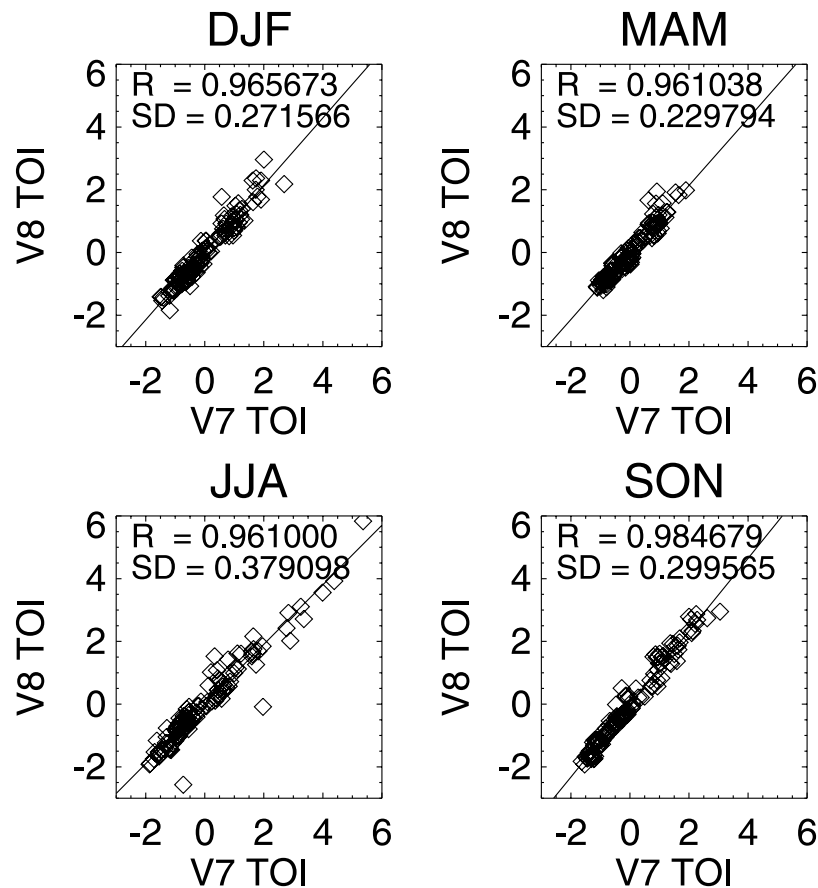
Figure 10. Comparison of tropospheric ozone index (TOI) residuals, which are the TOI values subtracted from zonal mean, from version 7 and version 8 TOMS data in four seasons. The R and SD represent the regression coefficient and standard deviation (one-sigma level).

the disagreement between ozone derived from satellite residual-based methods and the precursor distributions seen in both the fire count measurements and the MOPITT CO distributions in boreal winter and spring. We define this disagreement as the Northern Tropical Paradox.

[27] We have resolved this paradox with a new retrieval algorithm, the Scan Angle Method. This algorithm takes advantage of the difference in the TOMS retrieval efficiency between nadir and high viewing angles. The kernel for the difference is vertically broad in the troposphere with a maximum sensitivity centered at 5 km and thereby can be used as a surrogate for tropospheric ozone.

[28] We investigated the seasonality of fire counts, MOPITT CO concentrations, TOMS AI, ozone from the GEOS-CHEM model, and the CCD along with TOI from the SAM to analyze the ozone morphology. In meridional distribution, all products except the residual-based methods clearly reveal a seasonal oscillation that displays a maximum over northern tropical Africa in boreal winter and over southern tropical Africa in boreal summer. This seasonal oscillation was not observed by residual-based products including the tropospheric ozone residual method, modified-residual method, convective cloud differential, or clear cloudy pairs [*Fishman et al.*, 1990; *Martin et al.*, 2002; *Edwards et al.*, 2003; *Newchurch et al.*, 2003; *Ziemke et al.*, 1998]. The CCD product always finds the ozone maximum over the southern Atlantic off

the coast of southwest Africa. Investigation of in situ measurements from the MOZAIC campaign reveals the ozone maximum in boreal summer and the minimum in boreal winter at three locations over the northern tropics; Abidjan (5°N, 4°W), Madras (13°N, 80°E), and Bangkok (14°N, 101°E). The seasonality of the SAM and the model ozone are in accord with the MOZAIC, but the CCD ozone is about 6 months out of the phase. In zonal distribution, the SAM and the CCD products reveal persistently high ozone near the Atlantic and low ozone near central Pacific Ocean. A minor difference is that the SAM tropospheric ozone index and MOPITT CO show a local minimum over the Indian Ocean between Africa and the western Pacific Ocean, while the CCD ozone shows rather a gradual decreasing distribution from Africa to the western Pacific Ocean.

[29] We correct for the V7 errors associated with aerosols and seaglint effects in all our results and finally compare the TOI residuals (not DU) in zonal means as a function of season between V8 and corrected V7 data. The resulting differences between V8 and corrected V7 TOI are significantly smaller than the magnitude of the tropospheric ozone features discussed here.

Appendix A

[30] The GEOS-CHEM model was initially described by *Bey et al.* [2001]. Subsequent improvements are

described by *Martin et al.* [2002]. The model is driven by assimilated meteorological data updated every 3–6 hours from the Goddard Earth Observing System (GEOS) of the NASA Data Assimilation Office (DAO). We use for this study the GEOS data for 1996–1997, available with a resolution of 2° latitude by 2.5° longitude and 46 sigma levels in the vertical extending up to 0.1 hPa. For computational expedience we degrade the horizontal resolution to 4° latitude by 5° longitude and merge the vertical levels above the lower stratosphere, retaining a total of 26. We conduct simulations from March 1996 through November 1997. The first nine months are used to achieve proper initialization. We present results for December 1996 through November 1997.

[31] The GEOS-CHEM model includes a detailed description of tropospheric O_3-NO_x-hydrocarbon chemistry. It solves the chemical evolution of about 120 species with a Gear solver [*Jacobson and Turco*, 1994] and transports 24 tracers. Photolysis frequencies are computed using the Fast-J radiative transfer algorithm [*Wild et al.*, 2000], which includes Rayleigh scattering as well as Mie scattering by clouds and mineral dust. The tropopause in the model is determined using the World Meteorological Organization standard criterion of a 2 K km^{-1} lapse rate. The cross-tropopause transport of ozone is simulated by the Synoz (synthetic ozone) method [*McLinden et al.*, 2000] using their recommended flux of 475 Tg O_3 yr^{-1}.

[32] Emissions of NO_x from lightning are linked to deep convection following the parameterization of *Price and Rind* [1992] as implemented by *Wang et al.* [1998]. Biogenic isoprene and NO_x emissions from land are computed locally using modified versions of the *Guenther et al.* [1995] and *Yienger and Levy* [1995] algorithms, as described by *Wang et al.* [1998] and *Bey et al.* [2001]. Interannual variability in biomass burning emissions is determined from satellite observations as described by *Duncan et al.* [2003].

References

Bey, I., et al. (2001), Global modeling of tropospheric chemistry with assimilated meteorology: Model description and evaluation, *J. Geophys. Res.*, *106*, 23,073–23,096.

Chandra, S., J. R. Ziemke, P. K. Bhartia, and R. V. Martin (2002), Tropical tropospheric ozone: Implications for dynamics and biomass burning, *J. Geophys. Res.*, *107*(D14), 4188, doi:10.1029/2001JD000447.

Crutzen, P. J., and M. O. Andreae (1990), Biomass burning in the tropics: Impact on atmospheric chemistry and biogeochemical cycles, *Science*, *250*, 1669–1678.

Duncan, B. N., R. V. Martin, A. C. Staudt, R. M. Yevich, and J. A. Logan (2003), Interannual and seasonal variability of biomass burning emissions constrained by remote-sensed observations, *J. Geophys. Res.*, *108*(D2), 4100, doi:10.1029/2002JD002378.

Edwards, D. P., et al. (2003), Tropospheric ozone over the tropical Atlantic: A satellite perspective, *J. Geophys. Res.*, *108*(D8), 4237, doi:10.1029/2002JD002927.

Fishman, J., and J. C. Larsen (1987), Distribution of total ozone and stratospheric ozone in the tropics: Implication for the distribution of tropospheric ozone, *J. Geophys. Res.*, *92*, 6627–6634.

Fishman, J., C. E. Watson, J. C. Larsen, and J. A. Logan (1990), Distribution of tropospheric ozone determined from satellite data, *J. Geophys. Res.*, *95*, 3599–3617.

Galanter, M., H. Levy, and G. R. Carmichael (2000), Impacts of biomass burning on tropospheric CO, NO_x, and O3, *J. Geophys. Res.*, *105*, 6633–6653.

Guenther, A., et al. (1995), A global model of natural volatile organic compound emissions, *J. Geophys. Res.*, *100*, 8873–8892.

Horinouchi, T., F. Sassi, and B. A. Boville (2000), Synoptic-scale Rossby waves and the geographic distribution of lateral transport routes between the tropics and the extratropics in the lower stratosphere, *J. Geophys. Res.*, *105*, 26,579–26,592.

Hudson, R. D., and A. M. Thompson (1998), Tropical tropospheric ozone from total ozone mapping spectrometer by a modified residual method, *J. Geophys. Res.*, *103*, 22,129–22,145.

Jacobson, M. Z., and R. P. Turco (1994), SMVGEAR: A sparse-matrix, vectorized Gear code for atmospheric models, *Atmos. Environ.*, *28*, 273–284.

Jiang, Y., and Y. L. Yung (1996), Concentrations of tropospheric ozone from 1979 to 1992 over tropical Pacific South America from TOMS data, *Science*, *272*, 714–716.

Kim, J. H., and M. J. Newchurch (1996), Climatology and trends of tropospheric ozone over the eastern Pacific Ocean: The influences of biomass burning and tropospheric dynamics, *Geophys. Res. Lett.*, *23*, 3723–3726.

Kim, J. H., and M. J. Newchurch (1998), Biomass-burning influence on tropospheric ozone over New Guinea and South America, *J. Geophys. Res.*, *103*(D1), 1455–1461.

Kim, J. H., M. J. Newchurch, and K. Han (2001), Distribution of tropical tropospheric ozone determined directly from TOMS measurements, *J. Atmos. Sci.*, *58*, 2699–2708.

Li, Q., et al. (2001), A tropospheric ozone maximum over the Middle East, *J. Geophys. Res.*, *28*, 3235–3238.

Liu, X., M. J. Newchurch, and J. H. Kim (2003), Occurrence of ozone anomalies over cloudy areas in TOMS version-7 level-2 data, *Atmos. Chem. Phys. Discuss.*, *3*, 187–223.

Marenco, A., et al. (1998), Measurement of ozone and water vapor by Airbus in-service aircraft: The MOZAIC airborne program, an overview, *J. Geophys. Res.*, *103*, 25,631–25,642.

Martin, R. V., et al. (2002), Interpretation of TOMS observations of tropical tropospheric ozone with a global model and in situ observations, *J. Geophys. Res.*, *107*(D18), 4351, doi:10.1029/2001JD001480.

McLinden, C. A., S. C. Olsen, B. Hannegan, O. Wild, M. J. Prather, and J. Sundet (2000), Stratospheric ozone in 3-D models: A simple chemistry and the cross-tropopause flux, *J. Geophys. Res.*, *105*, 14,653–14,665.

McPeters, R. (2003), Earth Probe TOMS, TOMS Science Team Meeting, Boulder, Colorado.

Newchurch, M. J., D. Sun, and J. H. Kim (2001), Zonal wave-1 structure in TOMS tropical stratospheric ozone, *Geophys. Res. Lett.*, *28*, 3151–3154.

Newchurch, M. J., D. Sun, J. H. Kim, and X. Liu (2003), Tropical tropospheric ozone derived using clear-cloudy pairs (CCP) of TOMS measurements, *Atmos. Chem. Phys.*, *3*, 683–695.

Pochanart, P., J. Kreasuwun, P. Sukasem, W. Geeratithadaniyom, M. S. Tabucanon, J. Hirokawa, Y. Kajii, and H. Akimoto (2001), Tropical tropospheric ozone observed in Thailand, *Atmos. Environ.*, *35*, 2657–2668.

Price, C., and D. Rind (1992), A simple lightning parameterization for calculating global lightning distributions, *J. Geophys. Res.*, *97*, 9919–9933.

Scott, R. K., J.-P. Cammas, P. Mascart, and C. Stolle (2001), Stratospheric filamentation into the upper tropical troposphere, *J. Geophys. Res.*, *106*, 11,835–11,848.

Singh, H. B. (Ed.) (1995), *Composition, Chemistry, and Climate of the Atmosphere*, Van Nostrand Reinhold, Hoboken, N. J.

Thompson, A. M., and R. D. Hudson (1999), Tropical tropospheric ozone (TTO) maps from Nimbus 7 and Earth Probe TOMS by modified-residual method: Evaluation with sondes, ENSO signals, and trends from Atlantic regional time series, *J. Geophys. Res.*, *104*, 26,961–26,975.

Thompson, A. M., B. G. Doddridge, J. C. Witte, R. D. Hudson, W. T. Luke, J. E. Johnson, B. J. Johnson, S. J. Oltmans, and R. Weller (2000), A tropical Atlantic paradox: Shipboard and satellite views of a tropospheric ozone maximum and wave-one in January–February 1999, *Geophys. Res. Lett.*, *27*, 3317–3320.

Thompson, A. M., et al. (2003), Southern Hemisphere Additional Ozonesondes (SHADOZ) 1998–2000 tropical ozone climatology: 1. Comparison with Total Ozone Mapping Spectrometer (TOMS) and ground-based measurements, *J. Geophys. Res.*, *108*(D2), 8238, doi:10.1029/2001JD000967.

Wang, Y., D. J. Jacob, and J. A. Logan (1998), Global simulation of tropospheric O_3-NO_x-hydrocarbon chemistry: 1. Model formulation, *J. Geophys. Res.*, *103*, 10,713–10,726.

Waugh, D. W., and B. M. Funatsu (2003), Intrusions into the tropical upper troposphere: Three-dimensional structure and accompanying ozone and OLR distributions, *J. Atmos. Sci.*, *60*, 637–653.

Waugh, D. W., and L. M. Polvani (2000), Climatology of intrusions into the tropical upper troposphere, *Geophys. Res. Lett.*, *27*(23), 3857–3860.

Wild, O., X. Zhu, and M. J. Prather (2000), Fast-J: Accurate simulation of in- and below-cloud photolysis in tropospheric chemistry models, *J. Atmos. Chem.*, *37*, 245–282.

Yienger, J. J., and H. Levy (1995), Empirical model of global soil-biogenic NO_x emissions, *J. Geophys. Res.*, *100*, 11,447–11,464.

Yonemura, S., H. Tsuruat, S. Kawashima, S. Sudo, L. C. Peng, L. S. Fook, Z. Johar, and M. Hayashi (2002), Tropospheric ozone climatology over Peninsular Malaysia from 1992 to 1999, *J. Geophys. Res.*, *107*(D15), 4229, doi:10.1029/2001JD000993.

Ziemke, J. R., S. Chandra, and P. K. Bhartia (1998), Two new methods for deriving tropospheric column ozone from TOMS measurements: The assimilated UARS MLS/HALOE and convective-cloud differential techniques, *J. Geophys. Res.*, *103*, 22,115–22,128.

—————————————

J. H. Kim and S. Na, Department of Atmospheric Science, Pusan National University, 30 Jangjeon-dong, Geumjeong-gu, Busan 609-735, Republic of Korea. (jaekim@pusan.ac.kr)

R. V. Martin, Department of Physics and Atmospheric Science, Dalhousie University, Halifax, Nova Scotia, Canada B3H 4R2.

M. J. Newchurch, Atmospheric Science Department, University of Alabama in Huntsville, Huntsville, AL 35805, USA. (mike@nsstc.uah.edu)